JOURNAL OF SPACECRAFT AND ROCKETS
Vol. 33, No. 5, September–October 1996

Aerodynamic Analysis of Commercial Experiment Transporter Re-Entry Capsule

William A. Wood,* Peter A. Gnoffo,† and Didier F. G. Rault†
NASA Langley Research Center, Hampton, Virginia 23681-0001

An aerodynamic analysis of the Commercial Experiment Transporter re-entry capsule has been performed using the laminar thin-layer Navier–Stokes solver LAURA. Flowfield solutions were obtained at Mach numbers 1.5, 2, 5, 10, 15, 20, 25, and 27.5. Axisymmetric and 5-, 10-, and 20-deg angles of attack were considered across the Mach-number range, with the Mach 25 conditions taken to 90-deg angle of attack and the Mach 27.5 cases taken to 60-deg angle of attack. Finite-rate chemistry solutions were performed above Mach 10; otherwise, perfect-gas computations were made. Drag, lift, and pitching-moment coefficients were computed, and details of a wake flow are presented. The effect of including the wake in the solution domain was investigated, and base-pressure corrections to forebody drag coefficients were numerically determined for the lower Mach numbers. Pitching-moment comparisons were made with direct simulation Monte Carlo results in the more rarefied flow at the highest Mach numbers, showing agreement within 2%. Thin-layer Navier–Stokes computations of the axial force were found to be 15% higher than the empirical/Newtonian-based results used during the initial trajectory analyses.

Nomenclature

C_D	= drag coefficient
C_L	= lift coefficient
C_m	= pitching-moment coefficient
M	= Mach number
T	= temperature, K
V	= velocity, m/s
X, Y, Z	= Cartesian coordinates
α	= angle of attack, deg
γ	= ratio of specific heats
ρ	= density, kg/m^3

Subscript

∞	= freestream value

Introduction

THE Commercial Experiment Transporter[1,2] (COMET) is a new space enterprise to place small payloads in a microgravity environment for extended duration and return them to Earth. As a commercial enterprise, COMET was developed out of NASA's Centers for the Commercial Development of Space program.[3] Preliminary aerodynamic coefficients used during the design phase were determined from empirical correlations or modified Newtonian calculations by Hill and McCusker.[4] In conjunction with COMET's commercial developers and the U.S. Department of Transportation, which conducted a review as part of the return system licensing process, NASA undertook an independent mission safety assessment of the flight-configured re-entry capsule, performing trajectory and landing-footprint analyses.

In support of these trajectory analyses, the present study provided an improved aerodynamic data set for the COMET re-entry capsule throughout the hypersonic and supersonic flight regimes. Three-sigma uncertainties for the preliminary aerodynamics were estimated by McCusker and Hill[5] at 10–20%. The current study applies Euler and Navier–Stokes class algorithms, including reacting-flow gas chemistry, to obtain more comprehensive predictions for the lift, drag, and moment coefficients used to refine the dispersion analysis of the COMET re-entry capsule.

Configuration

The COMET re-entry capsule, pictured in profile in Fig. 1, is an axisymmetric design with a spherical heatshield of 1.22-m (48-in.) radius. The frontal diameter and area are 1.32 m (52 in.) and 1.37 m^2 (2124 in.^{2}), respectively, and are the nondimensionalizing length and area used in computing the aerodynamic coefficients. All moment coefficients reported here are referenced to a point on the axis of revolution 0.45 m (17.6 in.) back from the nose tip. An approximation to the true vehicle geometry was made on the base, which is modeled here as a flat disk connecting the sides with the rocket-nozzle cover. In reality, this region is recessed by approximately 4 in., providing stowage for the parachutes. The effect of this approximation is anticipated to be limited to very large angles of attack, where the recession would tend to produce a stronger restoring moment than predicted with the modeled geometry.

Algorithm

The LAURA code[6] was used to generate the computational aerodynamic predictions in the current study. LAURA is an upwind, point-implicit, second-order-accurate fluid dynamics solver based on an extension of the Roe flux-difference-splitting scheme.[7] The

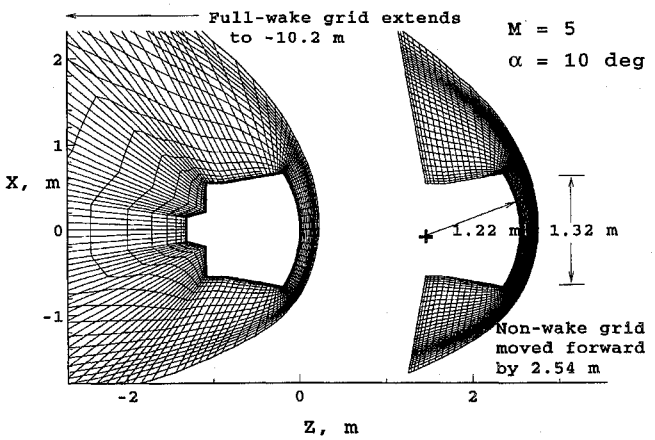

Fig. 1 Sample full-flowfield and nonwake symmetry plane grids, coarsened to show every other body-normal point.

Received Aug. 15, 1995; revision received May 23, 1996; accepted for publication May 26, 1996.

*Aerospace Technologist, Aerothermodynamics Branch, Gas Dynamics Division.

†Aerospace Technologist, Aerothermodynamics Branch, Gas Dynamics Division. Associate Fellow AIAA.

code has been developed to analyze the complete repertoire of hypersonic flow conditions on both slender and blunt vehicles and has been validated against Space Shuttle flight data by Weilmuenster and Gnoffo.[8] LAURA has previously been utilized in projects similar to the present study to analyze re-entry capsules for the Aeroassist Flight Experiment[9] and Mars Pathfinder Mission.[10]

Both Euler and laminar thin-layer Navier–Stokes solutions were obtained with LAURA about the COMET vehicle with perfect-gas and with seven-species, one- and two-temperature, finite-rate air. Steady-state assumptions were imposed. A plane of symmetry was assumed for three-dimensional solutions, and circumferential symmetry was assumed for axisymmetric solutions. The vehicle rotation, nominally 3 rpm at the atmospheric entry point, was not modeled.

Computational Grid

The computational grid used 64 cells in the body-normal direction, 36 cells circumferentially for the three-dimensional cases, and 66–72 cells down the body for the full-wake solutions. A close-up view of a full-wake-grid symmetry plane can be seen in the left half of Fig. 1. Calculations in the wake region assumed a laminar shear layer. Grids without wakes, seen on the right-hand side of Fig. 1, encompassed the forebody heat shield and vehicle sidewalls, back to the 90-deg corner where the base begins, 1.09 m (43 in.) from the nose. This breakpoint was chosen for the nonwake solutions because the flow typically undergoes a strong expansion at that point, limiting the upstream influence of the wake on the forebody flowfield. The grids were initially generated algebraically and then adapted as the solution evolved, aligning the grid with the bow shock and clustering points in the boundary layer.

Grid convergence was spot checked with respect to convergence of the vehicle aerodynamic coefficients. At Mach 25, 30-deg angle of attack, the viscous, seven-species, finite-rate-chemistry solution was obtained on $48 \times 12 \times 64$-, $95 \times 18 \times 64$-, and $95 \times 36 \times 64$-cell grids, counting streamwise, circumferentially, and normal to the body. Axial-force coefficients are within 1% on all three grids, and pitching-moment coefficients, compared to the finest-grid results, are within 3% on the coarsest grid and 1% on the intermediate grid.

Cases

An initial re-entry trajectory was defined by the POST[11] code based on the preliminary engineering approximations to the COMET aerodynamics. The capsule is expected to enter the rarefied atmosphere at approximately 70-deg angle of attack. A concurrent analysis of the rarefied aerodynamics determined that the COMET return capsule will weathercock into a heat-shield-first attitude by the time it reaches the continuum atmosphere, defined as Knudson numbers less than order one, or below 90 km for the COMET vehicle. A direct simulation Monte Carlo (DSMC) code[12] was utilized to provide the rarefied predictions. DSMC is currently considered to be the only practical technique with sufficient accuracy to realistically simulate very rarefied kinetics.

Thirty-six complete computational fluid dynamics solutions were obtained with LAURA at discrete Mach numbers ranging from 1.5–27 and an angle-of-attack range of 0–20 deg. The Mach 25 and 27 cases were taken to 90- and 60-deg angle of attack, respectively. The freestream conditions for each trajectory point are enumerated in Table 1, as well as a specification to whether the solutions were viscous or inviscid, with perfect-gas or reacting-air chemistry, and with or without the base-wake domain included in the calculations.

Results

Aerodynamic Coefficients

Drag, lift, and moment coefficients are compiled for the eight trajectory points at 0-, 5-, 10-, and 20-deg angle of attack in Table 2. Additional aerodynamics at Mach 25.4 and 27.5 for angles of attack greater than 20 deg are listed in Table 3. Drag data for 3 of the 36 cases have been corrected for base pressure effects, to be discussed in detail in the wake-effects section.

The COMET vehicle is at a maximum-drag condition about 0-deg angle of attack. The 0-deg-angle-of-attack drag coefficients vary between 1.55 at Mach 1.5 and 2, fall below 1.5 as the Mach number increases to 10, and then rise back to 1.55 by Mach 25 and above as the shock layer becomes more rarefied. Comparing drag coefficients with the more approximate methods used in Ref. 4 shows that the current results predict a 15% higher drag for COMET. The correspondingly lower ballistic coefficient indicates deceleration at higher altitudes and reduced downrange flight distance of the re-entry capsule relative to the preliminary design analyses.

Negative lift is generated by the free-flying capsule, expected by the very blunt configuration producing an axial force that dominates the normal force. The lift-curve slope is relatively constant between 0- and 20-deg angle of attack, at an average value of −0.015 per deg. The largest magnitude lift-to-drag ratio is −0.24 for Mach 20 and 20-deg-angle-of-attack conditions. At Mach 25 and 27, the vehicle returns to a zero-lift condition at 60-deg angle of attack. The Mach 25, 90-deg-angle-of-attack solution also has negative lift, though the data are too sparse in the 40–90-deg-angle-of-attack range to accurately define the lift trends.

Table 1 COMET trajectory points

M_∞	V_∞, m/s	ρ_∞, kg/m^3	T_∞, K	α, deg
1.51	451	38.4×10^{-3}	212	0,[b] 5,[a] 10,[b] 20[b]
2.00	601	26.8×10^{-3}	224	0,[b] 5,[a] 10,[b] 20[a]
5.06	1560	8.88×10^{-3}	236	0,[b] 5,[a] 10,[b] 20[a]
9.97	3200	3.12×10^{-3}	255	0,[b] 5,[a] 10,[a] 20[a]
15.1	5006	1.14×10^{-3}	271	0,[c] 5,[c] 10,[c] 20[c]
20.1	6429	431.0×10^{-6}	255	0,[c] 5,[c] 10,[c] 20[c]
25.4	7442	58.4×10^{-6}	213	0,[d] 5,[d] 10,[c] 20[d] 30,[d] 40,[d] 60,[d] 90[d]
27.5	7563	3.41×10^{-6}	187	0,[d] 20,[d] 40,[d] 60[d]

[a]Perfect gas, inviscid. [b]Perfect gas, viscous, wake included. [c]Reacting air, viscous. [d]Reacting air, viscous, wake included.

Table 2 COMET aerodynamic coefficients

		Angle of attack, deg			
M_∞		0	5	10	20
1.51	C_D	1.56	1.57	1.51	1.45
	C_L	0.0	−0.0586	−0.208	−0.266
	C_m	0.0	−0.0256	−0.0429	−0.0809
2.00	C_D	1.55	1.54	1.50	1.42
	C_L	0.0	−0.0734	−0.170	−0.233
	C_m	0.0	−0.0210	−0.0374	−0.0755
5.06	C_D	1.49	1.45	1.43	1.27
	C_L	0.0	−0.0882	−0.172	−0.280
	C_m	0.0	−0.0152	−0.0302	−0.0591
9.97	C_D	1.47	1.47	1.41	1.27
	C_L	0.0	−0.0912	−0.171	−0.291
	C_m	0.0	−0.0151	−0.0301	−0.0575
15.1	C_D	1.54	1.54	1.48	1.32
	C_L	0.0	−0.0929	−0.179	−0.312
	C_m	0.0	−0.0169	−0.0326	−0.0594
20.1	C_D	1.56	1.54	1.49	1.32
	C_L	0.0	−0.0981	−0.188	−0.320
	C_m	0.0	−0.0165	−0.0323	−0.0597
25.4	C_D	1.55	1.54	1.51	1.33
	C_L	0.0	−0.0962	−0.187	−0.310
	C_m	0.0	−0.0167	−0.0318	−0.0602
27.5	C_D	1.64	——	——	−1.45
	C_L	0.0	——	——	−0.262
	C_m	0.0	——	——	−0.0554

Table 3 COMET high-angle-of-attack aerodynamic coefficients

		Angle of attack, deg			
M_∞		30	40	60	90
25.4	C_D	1.12	0.997	0.923	0.994
	C_L	−0.341	−0.240	0.0137	−0.102
	C_m	−0.0868	−0.126	−0.139	−0.0923
27.5	C_D	——	1.25	1.26	——
	C_L	——	−0.247	−0.0117	——
	C_m	——	−0.143	−0.163	——

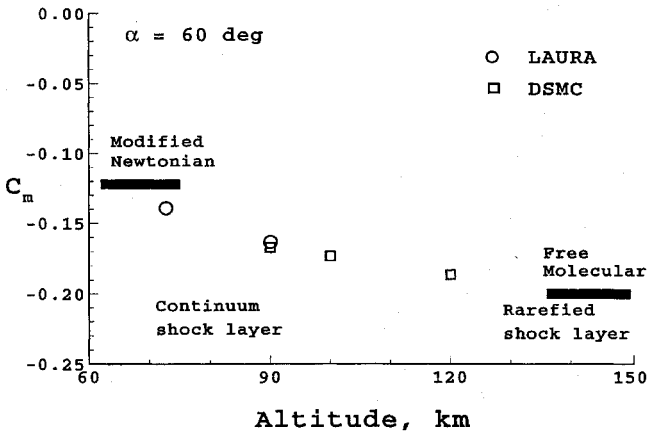

Fig. 2 Pitching moment coefficients at high altitudes.

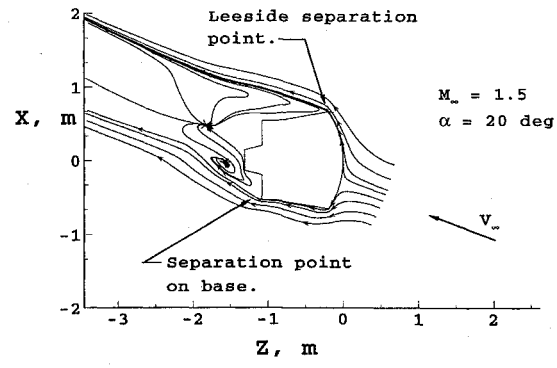

Fig. 3 Streamlines detailing wake recirculation region at Mach 1.5.

COMET is statically stable, with a negative pitching moment across the angle-of-attack range, trimmed at 0-deg angle of attack. The moment-coefficient slope has an average value of −0.0032 per deg between 0- and 40-deg angle of attack, nearly independent of Mach number. Beyond 60-deg angle of attack, the magnitude of the pitching moment decreases, though the moment is still negative so a restoring moment toward 0-deg angle of attack is maintained.

The variation in pitching-moment coefficient with altitude at 60-deg angle of attack is presented in Fig. 2. The altitudes range from the rarefied regime above 135 km, where the free-molecular calculation, following Bird,[13] is appropriate, through the transitional shock-layer conditions computed with the DSMC code, to the continuum results of LAURA. Very good agreement is seen between LAURA and DSMC at the overlap point at 90 km, where the DSMC moment coefficient differs by 2% from the LAURA prediction. The results of a modified Newtonian calculation, as from Anderson,[14] are included at the continuum altitudes for comparison and are seen to differ by 12% from the LAURA solution.

Wake Effects

Base-pressure corrections were made to the axial-force coefficient for three cases. The corrections were applied to compensate for neglecting the wake region in these solutions. For the Mach 1.5, 5-deg-angle-of-attack case, 0.24 was added to the axial-force coefficient. At Mach 2, the axial-force coefficients for both 5- and 20-deg angles-of-attack were increased by 0.16. These corrections were obtained from the 0- and 10-deg-angle-of-attack cases for Mach 1.5 and 2, which were computed both with and without the wake. At Mach 5, the difference between axial-force coefficients for solutions with and without wake computations was 0.02, or 1.3%. Above Mach 5, the difference between aerodynamic coefficients from solutions with and without wakes was negligible for small angles of attack. Base-pressure corrections were not made to the solutions that neglected the wake at Mach 5 and above.

Comparing the computed base-pressure corrections with those from a common engineering formula,[15]

$$\Delta C_{D,\text{base correction}} = \left(1/M_\infty^2\right) - \left(0.57/M_\infty^4\right) \qquad (1)$$

shows the LAURA corrections to be 24% smaller at Mach 1.5. Some of this difference is attributable to the LAURA grid extending around the forebody shoulder, including part of the afterbody.

At small angles of attack over most of the trajectory, the wake recirculation region is confined to the base of the vehicle, allowing for a forebody flowfield solution plus base-pressure correction to obtain the vehicle aerodynamics. At the lower Mach numbers, particularly Mach 1.5, and moderate angles of attack, the wake recirculation is not confined to the base of the vehicle, invalidating a base-pressure correction approach. Figure 3 shows a close-up view of the streamlines in the symmetry plane around the vehicle and in the wake for Mach 1.5, 20-deg-angle-of-attack conditions. The flowfield can be seen to separate on the leeside at the heat-shield shoulder. A large recirculation region in the wake extends from the base up and around the entire leeside of the vehicle. A three-dimensional structure in the wake can be seen in the source and sink toroidal vortex behind the vehicle. Fluid is entrained at the windside center of the vortex, located approximately 0.25 m (10 in.) behind the retrorocket nozzle. The fluid is pumped around the toroid and emerges in the symmetry plane as a source located at coordinates (−1.9, 0.5) in Fig. 3.

Effect of Gas Model and Viscosity

Perfect-gas solutions are computationally more efficient than the finite-rate-chemistry solutions, but experience indicates that the perfect-gas assumptions become less accurate in high-Mach-number flows. Overlap calculations with perfect-gas and finite-rate chemistry were made at Mach 5 and 10 axisymmetric conditions to assess the legitimacy of using the perfect-gas assumption for these conditions. At Mach 5, the reacting-flow drag coefficient is 0.6% higher than the perfect-gas result; at Mach 10, the reacting-flow drag is computed to be 2% higher than perfect-gas drag. These results are considered to substantiate the use of perfect-gas models with this configuration and trajectory for Mach numbers of 10 and below.

Overlaps were also made between viscous and inviscid perfect gas calculations for the axisymmetric, Mach 5 conditions. The inviscid drag coefficient, 1.462, is within 0.3% of the viscous result, 1.458. Both solutions neglected the base domain, as the postshock pressure on the heat shield is the dominant contributor to drag, and no separation at the shoulder was seen at this angle of attack.

Summary

Aerodynamic characteristics of the COMET re-entry capsule have been examined using the LAURA. Thin-layer Navier–Stokes and Euler solutions were obtained for eight trajectory points for Mach numbers between 1.5 and 27.5 and angles of attack from 0 to 90 deg. Both perfect-gas and finite-rate-air-chemistry models were employed. Axisymmetric drag coefficients varied from a low of 1.47 at Mach 10 to a high of 1.64 at Mach 27.5. Negative lift was generated at angles of incidence, with the lift coefficient varying between 0 and −0.32. The vehicle was statically stable, trimmed about 0-deg angle of attack, with a value of approximately −0.0032 per deg for $C_{m,\alpha}$ between 0- and 40-deg angle of attack. These results differ by 15% from the previously published data and are being used in refined landing-footprint analyses to ensure a safe splashdown location and to position the capsule recovery ship for swifter retrieval.

References

[1]Wessling, F. C., Robinson, M., Martinez, R. S., Gallimore, T., and Combs, N., "Commercial Experiment Transporter—COMET," *Journal of Spacecraft and Rockets*, Vol. 31, No. 5, 1994, pp. 846–854.

[2]Ajluni, T., and Hager, J., "Comet: Creating the United States' First Complete Commercial Space Service," AIAA Paper 92-1564, March 1992.

[3]Stone, B. A., "Space Commerce: Preparing for the Next Century," International Academy of Astronautics, IAA Paper 91-643, Montreal, PQ, Canada, Oct. 1991.

[4]Hill, S. M., and McCusker, T., "COMET Recovery System Flight Dynamics," AIAA Paper 93-3693, Oct. 1993.

[5]McCusker, T. J., and Hill, S. M., "Landing Dispersions for the Commercial Experiment Transporter Recovery System," AIAA Paper 93-3695, Nov. 1993.

[6]Gnoffo, P. A., "Point-Implicit Relaxation Strategies for Viscous, Hypersonic Flows," *Computational Methods in Hypersonic Aerodynamics*, edited by T. K. S. Murthy, Kluwer Academic, Norwell, MA, 1991, pp. 115–151.
[7]Roe, P. L., "Approximate Riemann Solvers, Parameter Vectors, and Difference Schemes," *Journal of Computational Physics*, Vol. 43, Oct. 1981, pp. 357–372.
[8]Weilmuenster, K. J., and Gnoffo, P. A., "Solution Strategy for Three-Dimensional Configurations at Hypersonic Speeds," *Journal of Spacecraft and Rockets*, Vol. 30, No. 4, 1993, pp. 385–394.
[9]Gnoffo, P. A., "Code Calibration Program in Support of the Aeroassist Flight Experiment," *Journal of Spacecraft and Rockets*, Vol. 27, No. 2, 1990, pp. 131–142.
[10]Mitcheltree, R. A., and Gnoffo, P. A., "Wake Flow about a MESUR Mars Entry Vehicle," AIAA Paper 94-1958, June 1994.
[11]Brauer, G. L., Cornick, D. E., and Stevenson, R., "Capabilities and Applications of the Program to Optimize Simulated Trajectories (POST)," NASA CR 2770, Feb. 1977.
[12]Rault, D. F. G., "Aerodynamics of the Shuttle Orbiter at High Altitudes," *Journal of Spacecraft and Rockets*, Vol. 31, No. 6, 1994, pp. 944–952.
[13]Bird, G. A., *Molecular Gas Dynamics*, Clarendon, Oxford, England, UK, 1976, pp. 80–106.
[14]Anderson, J. D., *Hypersonic and High Temperature Gas Dynamics*, McGraw–Hill, New York, 1989, pp. 53–56.
[15]Bonner, E., Clever, W., and Dunn, K., "Aerodynamic Preliminary Analysis System II. Part I—Theory," NASA CR 182076, April 1991.

T. C. Lin
Associate Editor